Chapter VII

Conclusions and future direction

The lanthanide series elements are best known for their optical and optoelectronic properties. Being environmentally stable system, the rare-earth oxides (REOs) have wide spread application in the manufacturing of high field tiny magnets, high performance luminescent devices, as well as in biomedical fields [1, 2]. The REOs display unique electronic, optical and luminescence properties that arise from the shielded *4f* electrons [3]. The RE sesquioxide Gd_2O_3 is a well-known, industrially relevant system owing to its superb thermal stability, chemical durability, high refractive index, etc. [4]. The lanthanide doped Gd_2O_3 nanometric systems have extended continuous attention for selective *D-F* mediated radiative emission followed by selection rule. This chapter includes highlights important conclusions drawn from the present investigation along with the relevance in future works.

This thesis is the outcome of structural, optical, optoelectronic, rheological and bio-physical characteristics of nanometric Gd_2O_3 systems. In particular, the effect of RE doping on the *D-F* transition mediated optical emission of gadolinium oxide and oxyfluoride systems are discussed. The Gd_2O_3 nanoparticles and rods are synthesized by adopting suitable physico-chemical and hydrothermal routes. The structural, optical and morphological characteristics of the synthesized samples were characterized through different characterization techniques. The structural characterization is performed by a Rigaku miniFlex X-ray diffractometer (XRD) that uses a copper target (CuK_α, λ=1.543Å). The diffraction intensity was monitored corresponding to the Bragg's diffraction angle (2θ) varied in the range of 20-60^o, while considering a scanning rate of 2^o/min and step angle of 0.05^o. Transmission electron microscopy (TEM) imaging was performed by a JEOL JEM 2100 machine or a TECNAI G2 20 S-TWIN machine, operating at an accelerating voltage of 200 kV. In HRTEM measurement, a sliced specimen was first dispersed in the DI water, and then subjected to ultra-sonication, for 1 h. A micro drop of the sample was placed on the carbon coated copper grid. The optical absorption study was performed by a UV-Visible spectrophotometer (UV 2450, Shimadzu), while luminescence response was explored by a PerkinElmer LS 55

spectrophotometer. The Raman spectra of the samples were recorded using a Renishaw In-Via Raman spectrometer (Renishaw, Wottonunder- Edge, UK) with an Ar^+ laser line (λ =514·5 nm) as the excitation source and with a detector resolution of 0.3 cm^{-1}. The electron paramagnetic resonance data have been acquired on a JEOL: JESFA200 EPR spectrometer. Lastly, magnetic hysteresis measurement was carried out at room temperature using a SQUID (Evercool SQUID VSM DC magnetometer, Quantum design, USA).

The optical properties of the pure and RE ion doped Gd_2O_3 and $Gd_4O_3F_6$ nanosystems are analyzed through optical absorption and photoluminescence (PL) spectroscopy studies. Intra *4f* transitions of Tb^{3+} and Eu^{3+} ions are recognized with various native defects in the host Gd_2O_3 and $Gd_4O_3F_6$. On the other hand, Judd-Ofelt (J-O) parameter of Eu^{3+} ions has been calculated from the emission spectra of Eu^{3+} doped $Gd_4O_3F_6$ nanosystems.

The impact of 80-MeV C^{6+} ion irradiation on the morphological, interrelated emission response and spin- spin relaxation features of the Gd_2O_3 nanorods are also discussed. Tamarind like shape deformation has been witnessed at a higher fluence due to multi ion impact mechanism. On increasing the irradiation fluence between 1×10^{11} and 3×10^{12} ions/cm^2, the emission associated with neutral oxygen vacancies (V_{Ox}), positioned at ~350 nm, underwent a steady increase as compared to that associated with the singly charged vacancies (V_O^+), located at ~414 nm. The enhancement of spin–spin relaxation time (τ_{ss}) is ascribed to a substantial changeover (from V_O^+ to V_{Ox} defects) with irradiation, V_O^+ being recognized as the major contributor to the paramagnetic centers [5].

The magneto-rheological behavior of the pristine and γ-irradiated Gd_2O_3 nanorod based MR fluids has been analyzed. The typical flow curve of our synthesized samples exhibited non-Newtonian characteristics. The rheological plots displayed a non-Newtonian power law ($\eta_v = K_v\dot{\gamma}^m$) behavior having power indices (m) varying in the range of 0.43–0.5. The apparent viscosity of the

fluids increased with increasing the magnetic field. A shear thickening to thinning jump has been also observed at a critical shear rate.

The cell-cytotoxicity assays, hemolytic against human RBCs analysis exhibit excellent biocompatibility of the Gd_2O_3 nanosystems. The prepared samples also inhibited the growth of HepG2 and MDA-MB231 cancer cells. Realizing a stronger impact by the latter cell type, the cell viability was observed to be significantly lowered, to an amount of ~65 and 57% on treatment with GNP and GNR systems (at 100 μg/mL); respectively. Moreover, the apoptotic analysis has been worked out for the aforesaid cell lines.

An effort is made to produce quality nanoscale Gd_2O_3 and Eu^{3+} doped $Gd_4O_3F_6$ systems. The work done in this thesis can be extended in many ways. One may consider following points to extend future research:

- Size and shape dependent response on magnetorheological and magneto-optic properties.
- Impact of swift heavy ion irradiation on structural, optical, morphological properties of Gd_2O_3 nanosystems for comparable electronic and nuclear energy losses can be studied.
- First principle calculations to explore structure property relationship in Gd_2O_3 system.
- Use of nanoscale Gd_2O_3 with different aspect ratios for application as MRI contrast agent.
- Cellular uptake process for both oxide and oxyfluoride nanosystems of different aspect ratios.

References

[1] Mornet, S., Vasseur, S., Grasset, F., and Duguet, E. Magnetic nanoparticle design for medical diagnosis and therapy. *Journal of Materials Chemistry*, 14: 2161-2175, 2004.

[2] Feng, J., Shan, G., Maquieira, A., Koivunen, M. E., Guo, B., Hammock, B. D., and Kennedy, I. M. Functionalized Europium Oxide Nanoparticles Used as a Fluorescent Label in an Immunoassay for Atrazine. *Analytical Chemistry*, 75: 5282-5286, 2003.

[3] Nichkova, M., Dosev, D., Gee, S. J., Hammock, B. D. and Kennedy, I. M. Microarray Immunoassay for Phenoxybenzoic Acid Using Polymer Encapsulated Eu:Gd_2O_3 Nanoparticles as Fluorescent Labels. *Analytical Chemistry*, 77:6864-6873, 2005.

[4] Guo, H., Dong, N., Yin, M., Zhang, W., Lou, L., and Xia, S. Visible upconversion in rare earth ion-doped Gd_2O_3 nanocrystals. *The Journal of Physical Chemistry B*, 108 : 19205–19209, 2004.

[5] Hazarika, S., and Mohanta, D. Interrelated emission and spin–spin relaxation feature mediated by V_O^+ defects in Gd_2O_3 nanorods subjected to swift ion impact. *Philosophical Magazine Letters,* 96:157–164, 2016.

Appendix I

Physical properties of gadolinium oxide (Gd_2O_3)

Molar mass	362.50 g/mol
Density	7.07 g/cm^3 (25 °C)
Solubility in water	Insoluble
Melting point	2420 °C
Crystal structure	Cubic Monoclinic Hexagonal
Lattice parameters (at 300 K)	a = 10.79 Å (Cubic) a= 14.06 Å, b=3.56 Å and c=8.76 Å (monoclinic) 3= 3.86 Å and c= 6.16 Å (hexagonal)
Refractive index	1.97
Band gap (at 300 K)	5.4 eV

Physical properties of gadolinium oxyfluoride ($Gd_4O_3F_6$)

Appearance	White odourless powder
Solubility	Soluble in acid
Structure	Tetragonal ($a_1 = a_2 \neq a_3$) Rhombohedral ($a_1 \neq a_2 \neq a_3$)

Appendix II

Physical properties of Ethanol

Molar mass	46.07 g/ml
Appearance	Colorless
Density	0.789 g/m3
Melting point	-114 C
Boiling point	78 C
Vapor pressure	5.95 kPa (at 293 K)
Acidity (pKa)	15.9
Basicity (pKb)	-1.9
Refractive index	1.36
Viscosity	0.0012 Pa.s (293 K)

Appendix III

Williamson-Hall expression

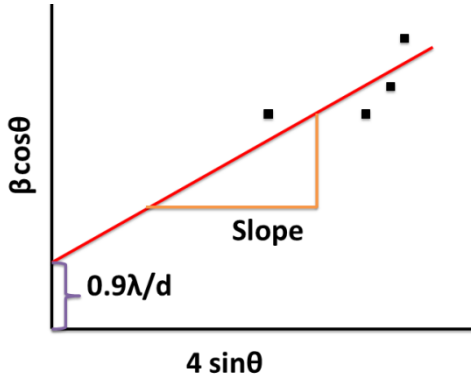

The average crystallite size (d) and microstrain (η) can be calculated from the Williamson-Hall (W-H) expression:

$$\beta \cos \theta = 0.9 \lambda / d + 4 \eta \sin \theta$$

where β is the full width at half maxima, θ is the Bragg diffraction angle in degrees, λ is the wavelength of X-ray (1.543 Å). Thus when we plot $\beta \cos \theta$ *vs.* $4 \eta \sin \theta$, get a straight line with slope η and intercept $0.9 \lambda / d$.

Characteristics of Non-Newtonian fluid

Sl. no	Non-Newtonian behaviour	Example
1	Shear thickening: Apparent viscosity increase with shear rate	Corn starch dissolved in water
2	Shear thinning: Apparent viscosity decrease with shear rate	Nail polish, Syrups
3	Thixotropic: Apparent viscosity decreases with time of constant shear	Gelatin gels, Paints

Appendix IV

Superconducting quantum interference device (SQUID)

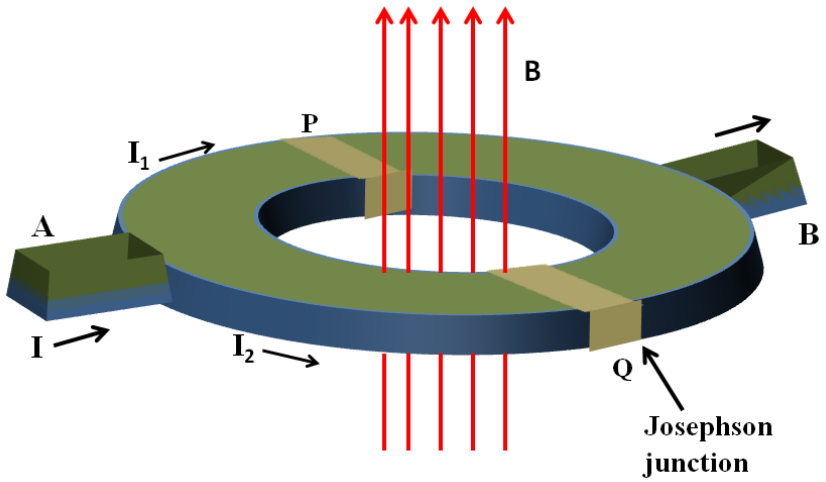

Figure: Schematic diagram of SQUID

SQUID magnetometer is one of the most effective and sensitive ways of measuring magnetic properties. The magnetometer consists of a ring of superconducting material with two side arms A and B which act as an entrance and exit for the supercurrent respectively and insulating layers P and Q [1]. These layers may have different thicknesses. Let the currents flowing through them are I_1 and I_2 respectively. They vary periodically with the magnetic field, with I_1 having greater periodicity. The variation of I_2 is an interference effect of the two junctions, whereas, diffraction is the cause for the variation of I_1, that arises from the finite dimension of each junction [1].

Reference

[1] Puri, R.K., and Babbar, V.K. *Solid state physics*, S.Chand &Company Ltd. ISBN:81-219-1476-0, 2003.

Appendix V

Ion irradiation experiment

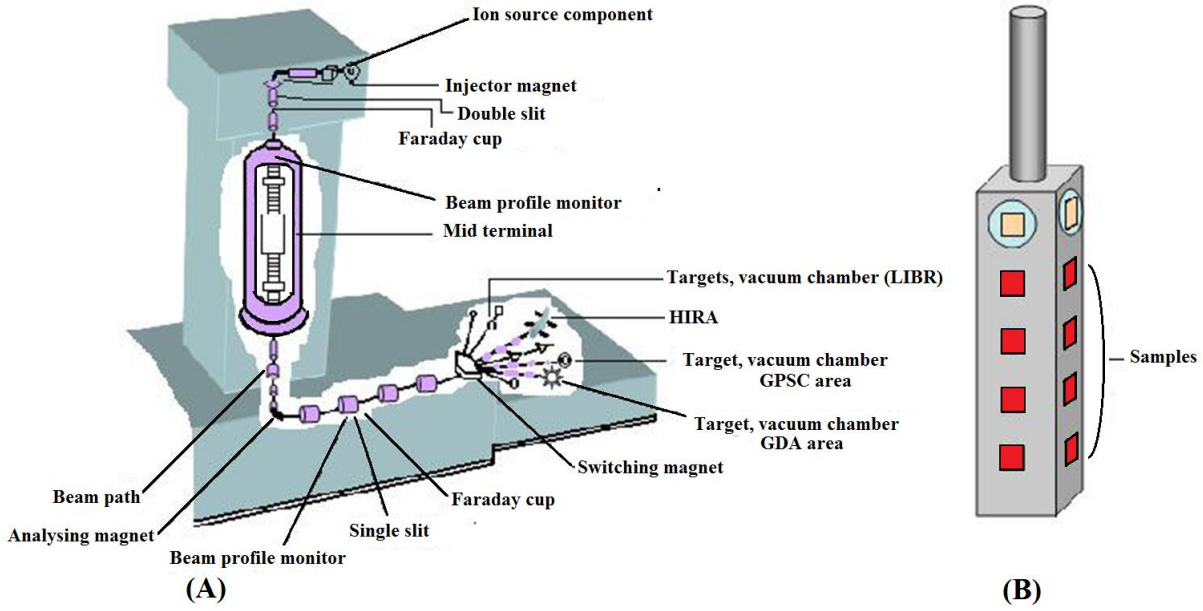

Figure : Schematic diagram of (A) the ion irradiation chamber and ion trajectory at Inter University Accelerator Center, New Delhi and (b) Ladder used to mount the samples in the vacuum chamber.

The high energetic ion beam experiment was performed at the 15UD Pelletron acceleration available at IUAC, New Delhi. Figure A depicts the schematic representation of the pelletron. In our present study the experiment were performed in the material science chamber by placing the samples in a ladder (Figure B). The movement of the ladder can be controlled as such to rotate and move up and down. At one time, 16-20 samples attached to the ladder can be irradiated without releasing the vacuum.

List of publications

1. S. Hazarika, D. Mohanta, Interrelated emission and spin–spin relaxation feature mediated by V_O^+ defects in Gd_2O_3 nanorods subjected to swift ion impact, *Philosophical Magazine Letters,* **96**, 157–164, 2016.

2. S. Hazarika, D. Mohanta, Oriented attachment (OA) mediated characteristic growth of Gd_2O_3 nanorods from nanoparticle seeds, *Journal of Rare Earths,* **34**, 158-165, 2016.

3. S. Hazarika, N. Paul, D. Mohanta, Rapid hydrothermal route to synthesize cubic-phase gadolinium oxide nanorods, *Bulletin of Materials Science,* **37**, 789–796, 2014.

4. S. Hazarika, D. Mohanta, Production and optoelectronic response of Tb^{3+} activated gadolinium oxide nanocrystalline phosphors, *The European Physical Journal Applied Physics,* **62**, 30401(p1-p5), 2013.

5. S. Hazarika, D. Mohanta, Sol-hydrothermally derived gadolinium oxide (Gd_2O_3) nanorods and tamarind-like shape evolution under 80 MeV C^{6+} ion impact, *Radiation effects and defects in solid*, **171**, 925-935,2016 .

6. S. Hazarika, D. Mohanta, Noticeable red emission and Raman active modes in nanoscale gadolinium oxyfluoride ($Gd_4O_3F_6$) systems with Eu^{3+} inclusion, *Applied physics A materials science and processing*, **123**, 382, 2017.